An Ab Initio Periodic Study of Acidic Chabazite as a Candidate for Dihydrogen Storage

F. J. Torres, B. Civalleri,* C. Pisani, and P. Ugliengo

Dipartimento di Chimica IFM, Università di Torino, and Nanostructured Interfaces and Surfaces, Centre of Excellence, Via P. Giuria 7, 10125 Torino, Italy

Received: February 9, 2006; In Final Form: April 7, 2006

A theoretical B3LYP study, adopting a polarized double-ζ quality Gaussian basis set, was performed to characterize acidic chabazite by using the periodic CRYSTAL03 program. Different Si/Al loadings (1/1, 3/1, 5/1, and 11/1) were considered, and for each of them the most stable aluminum distribution and location of the acidic proton, needed as charge balancer, were identified. With the optimal structures, the energy of formation and the anharmonic O−H stretching frequency were calculated with the latter being in good agreement with the experimental data. The B3LYP optimal position of H_2 physisorbed at the acidic Brönsted sites of chabazite (Si/Al = 11/1 and 5/1) brings about an interaction energy definitely smaller than that derived from infrared spectroscopy, because of the known deficiencies of this functional to cope with dispersive interactions. The latter was included by means of an ONIOM-like procedure that combines periodic B3LYP energy with results at the MP2 level on selected clusters cut out of the chabazite framework. Adsorption of two H_2 molecules for Si/Al = 5/1 chabazite showed a complete independence of each Brönsted site, and neither through-space nor intrastructure polarization effects are present. Within the periodic B3LYP approach shifts in both O−H and H−H anharmonic frequencies were also computed and compared with unperturbed values and with the available experimental results.

1. Introduction

The growing demand for fossil fuels around the world, their decreasing reserves, and the well-known environmental problems of these power sources demand the development of a suitable alternative to produce energy. In the last few years, intensive research has been dedicated to find a competitive resource[1,2] (in economical and commercial aspects), but the obtained results do not seem to be hopeful to date. Despite this, one promising option is the use of hydrogen as an energy carrier.[3−5] Its reaction with oxygen releases a relatively large quantity of energy with the additional advantage of producing water as a byproduct. Its generous distribution around the world, as part of compounds such as water and hydrocarbons, is another benefit of hydrogen, which can be extracted through suitable chemical transformations. The hydrogen-based economy has been divided into a set of three functional steps: production, storage, and use.[4,6] There are basic technical ways to achieve each of these mentioned steps, but none has been demonstrated to be very efficient. Of these predicaments, storage is possibly the most difficult problem to be solved.[7]

Among the proposed methods for hydrogen storage, molecular adsorption on microporous zeolitic materials has been proposed as a viable solution.[8−11] Interesting candidates for this purpose are Al-substituted chabazites,[12] which belong to the category of microporous aluminosilicate zeolites. This material is characterized by significant variations of the Si/Al ratio in its tetrahedral sites and by the presence of extraframework cations that are necessary to compensate for the effects of the substitution of silicon by aluminum atoms. When protons are used for this purpose, chabazite takes its acidic form (HCHA), and the resulting O−H groups are typical Brönsted sites. The structure consists of an infinite number of six-membered two-level rings that form hexagonal prisms that are oriented parallel to each other and perpendicular to the 3-fold axes. These facts permit us to classify chabazite into the ABC family where the prisms are arranged in three different levels along the *c*-axis.[13] This special distribution creates three-dimensional cages limited by 4 eight-membered, 2 six-membered, and 12 four-membered rings. The cavities have an approximate volume of 11 × 11 × 11 Å^3, and they are linked to each other through the eight-membered windows creating, in an infinite periodic expansion, a three-dimensional system of channels and cages[14,15] (Figure 1) in which hydrogen molecules may easily diffuse.

Recent experimental studies have suggested a relatively weak interaction with the Brönsted sites of the HCHA-11/1 structure. Zecchina et al.[8] reported a value of 9.7 ± 0.3 kJ/mol, which was obtained by using isobaric IR experiments performed at various temperatures. Spectra were recorded at decreasing temperatures in the range of 300−15 K under equilibrium conditions; meanwhile, a constant H_2 pressure was kept (57 mbar). The procedure permits measurement of the dependence of the bands related to the O−H···H_2 adducts in terms of temperature, from which the adsorption energy of H_2 on the Brönsted acidic sites can be quantified by using the Langmuir approximation and Van't Hoff equation.[16] The value of the interaction corresponds to the slope of the linear equation that correlates the equilibrium constant of the adsorption process (K_{ads}) with the inverse of the temperature ($1/T$).[17] However, the adopted method has not been demonstrated to be absolutely reliable and general, because it is necessary to consider within its accuracy the errors in the calculations of the integrated area of the IR bands and possible nonlinear behavior of the obtained data.

The purpose of the present work is to characterize by means of a periodic ab initio modeling approach the possible HCHA

* Author to whom correspondence should be addressed. E-mail: bartolomeo.civalleri@unito.it.

10.1021/jp060843y CCC: $33.50
Published on Web 05/11/2006

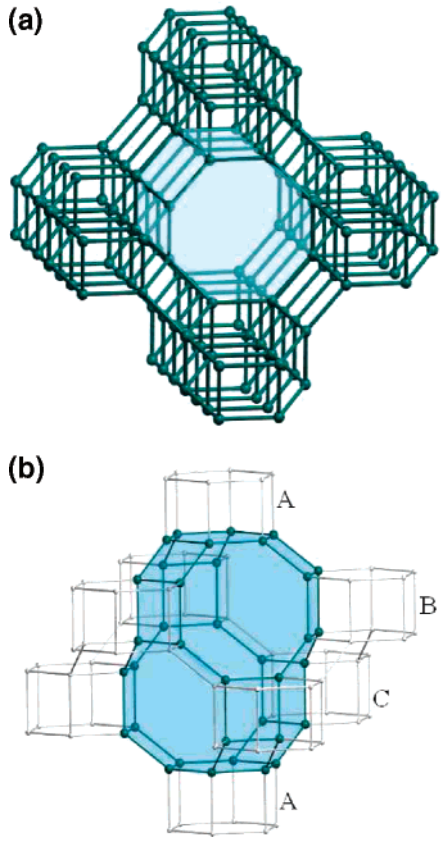

Figure 1. (a) Three-dimensional channel and (b) the schematic representation of the cage of all-silicon CHA. Oxygen atoms are excluded for a better appreciation of the structures.

systems for different Si/Al concentrations and, additionally, to understand and verify this relatively weak interaction of HCHA-11/1 and HCHA-5/1 (Al-substituted chabazite with Si/Al ratios of 11/1 and 5/1) with hydrogen molecules.

The structure of the paper is as follows: We first summarize the principal characteristics of the models and methods employed for the calculations in section 2. Section 3 contains the results and the discussion. It is divided in three main parts: (A) characterization of HCHA with variable Si/Al ratios, (B) study of the interaction between molecular hydrogen and HCHA-11/1, and (C) study of the interaction between hydrogen and the HCHA-5/1 system. In section 4, the main conclusions of the work are discussed.

2. Models and Methods

Pure silica chabazite, with a trigonal $R\bar{3}m$ space group, has a primitive cell composed of two 6-T rings linked in parallel (where a 6-T ring is defined as a ring that contains six tetrahedrally coordinated centers). The resulting hexagonal prism was used as the starting point for the generation of structures with variable Si/Al ratios. CHA-1/1, CHA-3/1, CHA-5/1, and CHA-11/1 were obtained by substituting with aluminum 6, 3, 2, and 1 silicon atoms in the cell, respectively. For each Si/Al ratio, different distributions of the Al atoms among the 12 equivalent vertexes of the hexagonal prism were determined. These must fulfill some empirical rules observed for zeolites (e.g., Lowenstein's rule which estabilished that Al−O−Al bridges are not permitted), so a total of 10 different cases are allowed: one case for both CHA-1/1 and CHA-11/1 and four cases for both CHA-3/1 and CHA-5/1 (Figure 2). The resulting point symmetry of these Al-substituted structures is obviously lower than that of all-silica chabazite, and it reduces to a *P*1 space group in most cases. As exposed in the previous section, chabazite zeolite takes its acidic form when protons are used to compensate for the negative net charges created by the Al substitutions. The hydrogen atom can be linked to one of the four available oxygen atoms bound to the Al atom, namely, O1, O2, O3, and O4 (Figure 3a), giving rise to four different Brönsted sites.

If both the Al distribution in the cell and the protonation sites are considered, then a large number of possible structures are obtained. With the objective to avoid a direct ab initio periodic description of all possible structures (which represents an enormous computational task), the geometries of each HCHA zeolite were preliminarily optimized by using the GULP[18,19] program. The GULP code has been demonstrated to produce excellent results in the prediction of inorganic crystal frameworks through lattice energy minimization.[20,21] This molecular mechanics technique uses a semiclassical shell ion model potential. In this work, potential functions derived from ab initio B3LYP calculations for aluminosilicates[22] were used instead of the traditional empirical ones. In the following, the results obtained at this level will be referred as GB3. To further reduce the number of calculations, in the cases where more than just one substitutional Al atom is present, all protonation sites have been forced to occur at the same framework oxygen for each Al position (either O1 or O2, etc.). The notation O2O2′, O3O3′, etc., adopted throughout the paper, means that one proton is bound to oxygen 2 of the first Al atom and the other proton to oxygen 2 of the oxygen shell of the second Al atom. The results of this first stage run allow us to identify the most stable structures for each Si/Al ratio, which were subsequently fully reoptimized with the periodic ab initio CRYSTAL03 software package.[23] With this code, the long-range electrostatic effects (neglected in cluster models commonly adopted for zeolites' modelling) are rigorously taken into account by fully exploiting the Ewald summation in the three lattice directions. For the present theoretical study, a development version of the program was employed. All-electron basis sets were adopted, with 31G-(p), 6-21G(d), 6-31G(d), and 8-511G(d) contractions for H, Si, O, and Al, respectively. The exponents (in $bohr^{-2}$ units) of the most diffuse shell were optimized for the HCHA ($\zeta_{sp}(Si) = 0.13$, $\zeta_{sp}(O) = 0.27$, and $\zeta_{sp}(Al) = 0.28$); the exponents of the polarization functions are $\zeta_p(H) = 1.1$, $\zeta_d(Si) = 0.5$, $\zeta_d(O) = 0.6$, and $\zeta_d(Al) = 0.47$. CRYSTAL03 determines the equilibrium atomic positions by using a modified conjugate gradient algorithm very similar to that proposed by Schlegel[24] for molecular cases. The convergence for the geometry optimization is tested on the root mean square (RMS) and the absolute value of the largest component of the gradients and nuclear displacements. The thresholds for the maximum and the RMS forces and the maximum and RMS atomic displacements were set to 0.00045, 0.00030, 0.0018, and 0.00120, respectively (values in a.u.). When the four conditions are satisfied simultaneously, the optimization process is considered complete.[25] For all the calculations, the B3LYP Hamiltonian was used.[26] It contains a hybrid Hartree−Fock (HF)/density functional exchange−correlation term. This Hamiltonian is commonly and successfully used in molecular quantum chemistry and in solid-state calculations.[27] Its results for structural and vibrational properties are excellent especially when O−H groups are involved.[28] Additionally, B3LYP with similar basis sets has also been successfully adopted by some of us to model the CO interaction with the HCHA-11/1 structure.[29] The results obtained at this level will be referred as B3LYP in the rest of the paper.

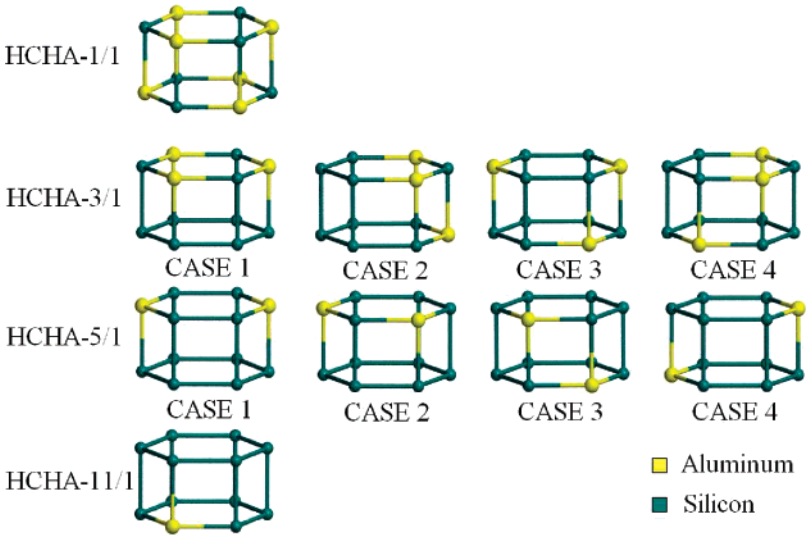

Figure 2. Aluminum distribution in the CHA hexagonal prism with different Si/Al ratios. H an O atoms are not considered in the graphic.

For the optimized geometries, the calculation of the anharmonic O−H stretching frequency was performed, by considering the O−H bond as an independent oscillator. The total potential energy is calculated at seven points that correspond to variations in the bond length ($\Delta_{O-H} = -0.2, -0.16, -0.06, 0.00, 0.16, 0.24$, and 0.30 Å), and a polynomial curve of the sixth degree is used to fit the energy points. The anharmonic constant ($\omega_e x_e$) and the harmonic O−H stretching frequency (ω_e) are computed from the first vibrational transitions ω_{01} and ω_{02} obtained by solving numerically the one-dimensional Schrödinger equation[30]

$$\omega_e x_e = \frac{2\omega_{01} - \omega_{02}}{2}$$

$$\omega_e = \omega_{01} + 2\omega_e x_e$$

For the study of the interaction between H_2 and the zeolites, three periodic models were considered, H_2−HCHA-11/1, H_2−HCHA-5/1, and $2H_2$−HCHA-5/1, which correspond to the addition of one molecule per unit cell for the two first cases and two molecules per unit cell for the last one. By considering that the interaction energy is rather small and to save computer time, the geometries of the H_2−HCHA systems were optimized by keeping the HCHA framework fixed at its free geometry while allowing the acidic Brönsted proton and the whole H_2 molecule to fully relax their positions. The calculation of the binding energies between each acidic zeolite and molecular hydrogen were worked out according to the supermolecular approach

$$BE_{[H_2-HCHA]} = E_{[HCHA]} + E_{[H_2]} - E_{[H_2-HCHA]}$$

All values were corrected for basis set superposition error (BSSE) by using the Boys−Bernardi full counterpoise method.[31] The resulting values will be to referred as BE_c.

Since present density functional theory functionals cannot cope with dispersive interactions[32−34] a more appropriate scheme was tested for describing the interaction of H_2 with the zeolites by using the ONIOM2 approach.[35] It subdivides the system in two parts or layers that are described at different levels of theory: The former layer denoted the *real system*, in the present work, is the whole periodic structure; the latter, the *model system*, is a fraction of the former, and it contains the Brönsted sites and the hydrogen molecule. The construction of the model system is done by cutting out a zone of the whole structure and by adding fictitious atoms (hydrogen atoms) in the case where covalent bonds are broken. Recently, this approach has been successfully adopted to include dispersive contributions to the interaction of CO with the (001) face of a MgO crystal.[36] Selected clusters for H_2−HCHA-11/1 and $2H_2$−HCHA-5/1 are shown in Figure 4. The ONIOM2 definition of energy $E_{[high:low]}$ is

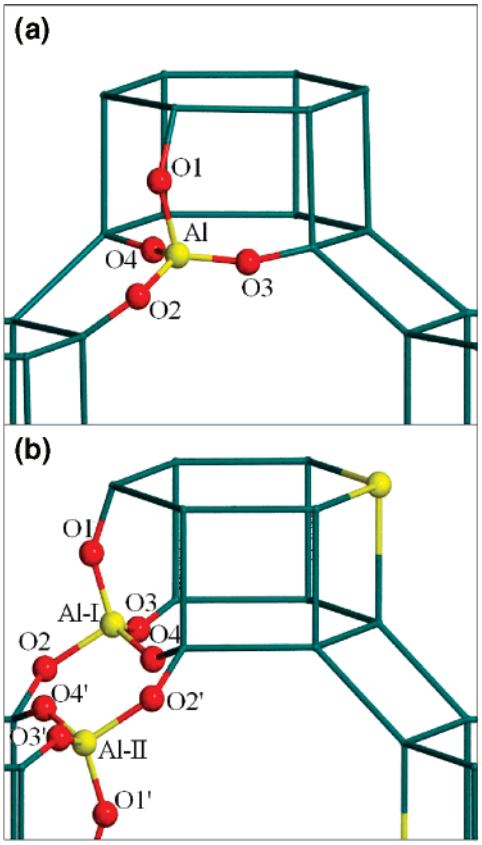

Figure 3. Protonation sites (a) in the structure of HCHA-11/1 and (b) in the structure of HCHA-5/1.

$$E_{[high:low]} = E_{[high,model]} + E_{[low,real]} - E_{[low,model]}$$

Here, $E_{[high,model]}$, $E_{[low,real]}$, and $E_{[low,model]}$ are the total energies computed on the model system with the high level of theory and on both the real and the model systems with the low level

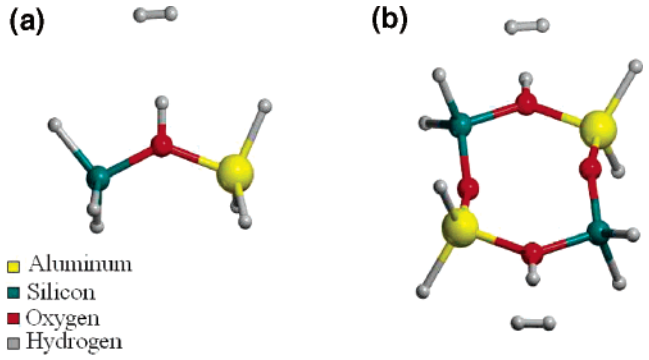

Figure 4. Model systems used in the ONIOM2 approach for (a) HCHA-11/1 and (b) HCHA-5/1.

of calculation. In the present work, the low level of theory corresponds to the B3LYP hybrid functional already described above, whereas the MP2 method[37] was adopted as the high level together with two aug-cc-VDZ and aug-cc-VTZ[38] basis sets to accurately compute dispersive interactions. All MP2 calculations were carried out with the molecular ab initio code Gaussian.[39] This kind of combination between (i) the very large basis set containing both multiple sets of polarization and diffuse functions and (ii) the correlated post-self-consistent field (SCF) method based on expansion of the wavefuntion ensures the dynamical electron correlation responsible for dispersion forces to be properly taken into account.[36] Additionally, the ONIOM2 formulation makes certain that if the low level of calculation is improved to reach the higher adopted level or if the model system is enlarged to become the real system, then it should result in $E_{[high:high]} = E_{[high:real]}$.

3. Results and Discussion

A. Characterization of HCHA with Variable Si/Al Ratios. As described in the previous section, the first stage of our study consisted of the geometrical optimization, with the GULP program, of all possible structures in terms of (i) allowed distribution of Al atoms and (ii) the position of the protonation site for a given Si/Al ratio. The considered "cases" are depicted in Figure 2. Among all systems with the same stoichiometry (i.e., the same Si/Al ratio) the most stable structure S_0 was identified and taken as a reference; for all the others, the difference in stability with respect to S_0 was calculated as RS $= E(S) - E(S_0)$. The results are reported in Table 1. To avoid a too large dataset for the Si/Al ratios 3/1 and 5/1 the protonation has been assumed to occur at the same oxygen for each aluminum substitution, i.e., O1O1′, O2O2′, and so on (Figure 3).

The most stable GB3 structures (those with RS = 0) are 1/1-O1, 3/1-case2-O1, 5/1-case4-O4, and 11/1-O1. For all others, the average value of RS is 42 kJ/mol, with a maximum instability of 83 kJ/mol (3/1-case1-O2). The favored protonation positions are generally O1 and O4, with some exceptions.

As already explained in the Models and Methods section, most of the structures were reoptimized in a further stage by using the program CRYSTAL03 taking as a starting point the corresponding GB3 geometries. We only disregarded, for each of the four cases corresponding to Si/Al ratios of 3/1 and 5/1, the two protonation sites that had resulted in the most unstable ones from the GULP calculations. For the remaining reoptimized 24 structures, the value of RS was determined as before, and the results are collected in Table 1. It is noteworthy that the order of stability practically coincides with that of the GB3 set, although the B3LYP values of RS tend to be smaller.

TABLE 1: Relative Stabilities (RS) of the HCHA Zeolites Calculated with the GULP and CRYSTAL03 Programs[a]

		relative stability			
zeolite	Al distribution case	O1	O2	O3	O4
	GB3 Level				
HCHA-1/1		0.00	18.84	65.32	35.51
HCHA-3/1	case 1	32.11	82.97	43.57	60.92
	case 2	0.00	40.43	31.01	75.57
	case 3	12.18	61.41	76.44	34.59
	case 4	25.34	33.37	15.92	79.34
HCHA-5/1	case 1	23.88	34.50	46.08	37.40
	case 2	42.73	52.27	68.31	65.38
	case 3	31.66	40.93	29.38	71.59
	case 4	42.33	22.69	41.34	0.00
HCHA-11/1		0.00	15.78	10.60	16.85
	B3LYP Level				
HCHA-1/1		0.00	14.29	71.14	22.25
HCHA-3/1	case 1	22.92		39.87	
	case 2	0.00		10.70	
	case 3	21.73			38.42
	case 4	41.66		26.22	
HCHA-5/1	case 1	28.68	57.69		
	case 2	28.85	42.27		
	case 3	44.16		22.01	
	case 4		16.2		0.00
HCHA-11/1		0.00	10.40	5.30	10.52

[a] The systems with RS = 0.00 correspond to the most stable structure (S_0) for each Si/Al ratio (see the text for details). All the energy differences are in kJ/mol.

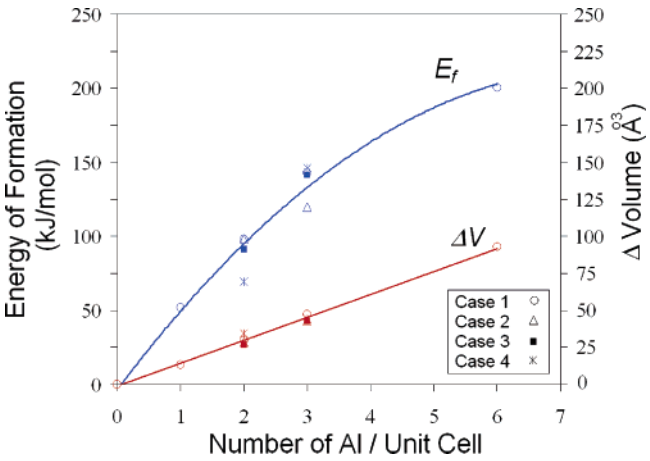

Figure 5. Change in cell volume and formation energy per unit cell of the various HCHA structures as a function of the number of substitutional Al sites per cell. See text for the definition of the energy of formation (E_f).

The geometrical and energetic effects caused by the different Al loadings in the unit cell are shown in Figure 5. Only the B3LYP data are used, and for each Al distribution, only the protonation site corresponding to the maximum stability has been included. Concerning the geometrical aspects, an increment of the cell volume was predicted when the Al content increases. This is an expected consequence of the larger size of the Al atoms with respect to the framework Si atoms. As for the energetic aspects, the *formation energy* (E_f) of the different chabazites has been computed by making reference to the all-silica CHA ($(SiO_2)_{12}$), α-Al_2O_3 corundum phase, and molecular water, according to the reaction

$$\frac{x}{12}(SiO_2)_{12} + \frac{y}{2}[Al_2O_3 + H_2O] \rightleftharpoons (SiO_2)_x(AlO_2H)_y$$

$$E_f = E_{(SiO_2)_x(AlO_2H)_y} - \frac{y}{2}[E_{\alpha-Al_2O_3} + E_{H_2O}] - \frac{x}{12}E_{(SiO_2)_{12}}$$

The best fit curve of Figure 5 shows that the energetic cost of the inclusion of an additional substitutional atom gradually decreases with the increasing Al concentration; i.e., Al atoms are accommodated more easily in the hexagonal prism if at least one is already present in the framework.

The anharmonic vibrational O−H stretching frequency, related to the acidity of the zeolites,[40] was evaluated in a further step. Table 2 shows the O−H distances and the O−H group vibrational properties for the structures optimized at the B3LYP level. It is worth noting that no correlation exists between the O−H bond length and the associated frequency. The reason may be due to the different local environments of the proton in the framework and to the influence on the frequency value of the long-range electrostatic field. The acidic properties of HCHA-11/1 were recently studied by IR spectroscopy,[8,15,41] allowing for a comparison with the present theoretical results. An IR experimental spectrum shows two main peaks at 3584 (LF) and 3616 (HF) cm^{-1}, with the second one being the most intense. The calculated ω_{01} frequencies are higher than the experimental ones, but some dependence on the basis set quality is expected. As reported by Civalleri et al.,[42] a decrement of 20 cm^{-1}, in the O−H stretching frequency, was observed when passing from B3LYP/DZP to B3LYP/aug-cc-pVDZ on cluster models of the Brönsted site. By application of the same correction to the present results, the values of 3635, 3618, 3627, and 3600 cm^{-1} for the ω_{01} frequency are obtained, respectively, for positions O1, O2, O3, and O4, in better average agreement with the experimental values. From Table 1, protonation sites at O1 and O3, for HCHA-11/1, are the most stable ones, and the O−H stretching values of 3635 and 3627 cm^{-1} differ only by 8 cm^{-1} compared to the value of about 33 cm^{-1} resulting from experiments.[15,41] The HF band corresponds to the most exposed Brönsted sites,[41] that is O1 and O3 in this case, which have similar O−H stretching frequencies; the LF band could be assigned to the protonation sites in the six-membered ring, i.e., O4. The difference computed between the O1(O3) O−H stretching values and the O4 one is around 30 cm^{-1}, confirming the interpretation above.

B. Interaction of Molecular Hydrogen with HCHA-11/1. For the construction of the H_2−HCHA-11/1 periodic model, a hydrogen molecule was introduced in the cavity of the framework, close to the polarizing centers that correspond to the extraframework protons (Figure 6). H_2 can interact with the adsorption sites through dispersion forces, electrostatics, and orbital interactions, as recently described by Lochan and Head-Gordon.[43] In this case, along with dispersion forces, electrostatics should play an important role via polarization and quadrupolar interactions. The position of the hydrogen molecule inside the zeolite cavity was computed keeping the framework atoms fixed at their position in the free zeolite, allowing the acidic proton and the H_2 molecule to be fully optimized. The corresponding results are summarized in Table 3. In all cases, the distances between the center of mass of the H_2 molecule and the acidic proton ($d_{H\cdots H_2}$) are close to 2.0 Å. It also appears that the O−H distance slightly increases in most cases, except for position O4. A possible explanation for such behavior is that, in pure HCHA-11/1, the O4−H is located inside the six-membered ring experiencing a weak interaction with the surrounding oxygen atoms. Even if such an intramolecular interaction is weak it is however stronger than that enjoyed with the H_2 molecule, so that the O−H bond length decreases slightly in correspondence to the increment of 20° degrees in the Si−O(H)−Al torsion angle due to the interaction with H_2.

TABLE 2: Optimal Bond Lengths and Fundamental ω_{01}, First Overtone ω_{02}, Harmonic ω_e, and Anharmonic Constants $\omega_e x_e$ for the O−H Group in the Structures Optimized at the B3LYP Level[a]

zeolite	Al distribution	proton position	d_{OH}	ω_{01}	ω_{02}	ω_e	$\omega_e x_e$
HCHA-1/1		O1	0.9753	3703	7253	3856	77
		O4	0.9689	3698	7245	3849	76
HCHA-3/1	case 2	O1	0.9696	3709	7264	3865	77
		O3	0.9724	3669	7185	3824	77
HCHA-5/1	case 4	O2	0.9701	3699	7243	3855	78
		O4	0.9750	3617	7077	3774	78
HCHA-11/1		O1	0.9695	3655	7151	3816	80
		O2	0.9715	3638	7123	3791	77
		O3	0.9742	3647	7139	3803	78
		O4	0.9754	3620	7085	3776	78

[a] For HCHA-3/1 and HCHA-5/1 zeolites, only the most stable cases of aluminum distribution are reported. Distances are in angstroms, and frequencies in cm^{-1}.

The perturbation of the O−H frequency due to H_2 interaction and, in turn, that of the H−H stretching frequency due to the acidic proton have been analyzed, and the results are reported in Table 3. A bathochromic shift is computed for the stretching frequencies of the O1−H, O2−H, and O3−H bonds. On the contrary, a computed hypsochromic shift results for the O4−H case due to the peculiar behavior of this proton site already explained above. The frequency shift ($\Delta\omega_{01}$) for the most stable proton position O1 is slightly overestimated with respect to the measured values[8] (−70 cm^{-1}). With regard to H_2 frequency shifts, they span the 50−70 cm^{-1} range. Unfortunately, the experimental determination of the H_2 shifts is hindered by the complexity of the band shape in the region of interest, which makes a proper comparison between theoretical and experimental data difficult.

The BSSE-corrected binding energies (BE_c in Table 3) are much smaller than the suggested experimental result of 9.7 kJ/mol.[8] This fact was expected, because the adopted Hamiltonian cannot properly cope with very weak intermolecular interactions in which dispersion contribution plays a major role[32] as in the present case. When the ONIOM2(MP2:B3LYP) approach, as described in the Models and Methods section, is applied to the case where the Brönsted proton is the most accessible one, as for the O1 case, the BE_c values amount to 4.7 and 5.2 kJ/mol, for aug-cc-pVDZ and aug-cc-pVTZ basis sets, respectively. Despite this correction, the present values are still about half of the one reported from experiment.[8]

C. Interaction of Molecular Hydrogen with HCHA-5/1. HCHA-5/1 was also considered for the study of the interaction with molecular hydrogen because of the following reasons: (a) the presence of two close in space protons in the structure could increase the interaction with the H_2 molecule; (b) the computed energy of formation which shows that HCHA-5/1 is only slightly less stable than HCHA-11/1 ($\Delta E_f \approx 17.7$ kJ/mol), so it may be present in the experimental sample.

The interaction with H_2 has only been considered for case 4 (Figure 2), in which the two substitutional Al atoms are at the opposite ends of the hexagonal prism. This structure is by far the most stable among the Si/Al ratio of 5/1 as shown in Table 1. For the present system, two protons are needed to compensate for the effect of the double Al substitution in the zeolite

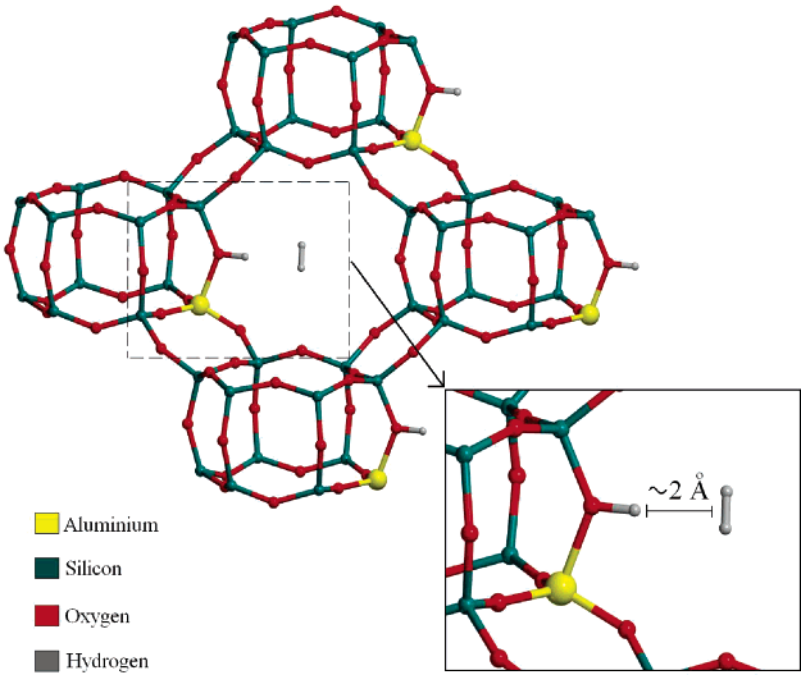

Figure 6. Hydrogen molecule inserted in the HCHA-11/1 cavity. The extraframework proton is positioned in O1.

TABLE 3: Optimized Distances between the H_2 Center of Mass and the Proton Site ($d_{H\cdots H_2}$), BSSE-Corrected Binding Energies (BE_c), and Changes in the O−H Bond Distances and the O−H and H−H Fundamental Stretching Frequencies for Each Brönsted Site of the HCHA-11/1 Zeolite[a]

proton position	$d_{H\cdots H_2}$	BE_c	O−H bond				H−H bond	
			d_{OH}	Δd_{OH}	ω_{01}	$\Delta\omega_{01}$[b]	ω_{01}	$\Delta\omega_{01}$[c]
O1	2.0214	1.2	0.9728	0.0033	3565	−90	4174	−64
O2	2.0439	0.8	0.9746	0.0031	3556	−82	4171	−67
O3	2.0143	1.4	0.9770	0.0028	3568	−79	4182	−56
O4	2.1475	1.8	0.9729	−0.0025	3628	+8	4188	−50

[a] Distances are in angstroms, BE_c in kJ/mol, and frequencies and shifts in cm^{-1}. [b] For the O−H bond $\Delta\omega_{01}$ is defined by the difference: $\omega_{01}^{OH}{}_{[H_2-HCHA-11/1]} - \omega_{01}^{OH}{}_{[HCHA-11/1]}$. [c] For the H−H bond $\Delta\omega_{01}$ is defined by the difference: $\omega_{01}^{HH}{}_{[H_2-HCHA-11/1]} - \omega_{01}^{HH}[H_2]$.

framework. Therefore, eight different Brönsted sites resulted in the structure, O1, O2, O3, and O4, belonging to Al in the upper six-membered ring (Al-I), and O1′, O2′, O3′, and O4′, belonging to Al in the lower six-membered ring (Al-II), as shown in Figure 3b. As remarked in section 3.A, only the structures protonated in the same position for both aluminum atoms were considered until this point (i.e., O1O1′, O2O2′, and so on). However, for a more thorough understanding of the H_2 adsorption mechanism, all possible combinations of the topologically different Brönsted sites have been considered in the following. To avoid a costly ab initio description of all possibilities, the adopted procedure was the same as that used for the global structural characterization. After prescreening the free HCHA-5/1 structures at the GB3 level, only the five most stable cases (O1O4′, O2O2′, O3O2′, O3O4′, and O4O4′) were selected for the subsequent ab initio periodic calculation at the B3LYP level. The results are reported in Table 4. The order of relative stability, for the five combinations, is: O4O4′ > O2O2′ >O1O4′ > O3O2′ ≈ O3O4′ with O4O4′ being well separated from the other cases. In the same table, the values of the calculated anharmonic O−H stretching frequencies are shown, also covering cases that have not been taken into account in section 3.A.

TABLE 4: Relative Stabilities (RS), Optimal O−H Bond Lengths, and Fundamental O−H Strretching Frequencies ω_{01} for the Five Most Stable Combinations of Brönsted Sites in HCHA-5/1 Zeolite[a]

combination	RS	Al-I set		Al-II set	
		d_{OH}	ω_{01}	d_{OH}	ω_{01}
O1O4′	28.7	0.9708	3665	0.9735	3634
O2O2′	16.2	0.9701	3699	0.9701	3699
O3O2′	33.1	0.9753	3647	0.9713	3640
O3O4′	33.5	0.9733	3664	0.9755	3622
O4O4′	0.0	0.9750	3617	0.9750	3617

[a] Relative stabilities are in kJ/mol, distances in angstoms, and frequencies in cm^{-1}.

For the simulation of the H_2−HCHA-5/1 system, one hydrogen molecule per unit cell was added to each of the five systems, and its influence on the local Brönsted geometry was analyzed. In all cases the hydrogen molecule stays preferably close to one of the two available Brönsted sites, allowing the second one to be completely free of interaction. As a consequence, significant changes in the O−H bond distance were only computed for the O−H group belonging to the Al-I set (as reported in Table 5). In almost all cases, a small O−H bond distance lengthening is computed, except for the hydrogen molecule in interaction with the proton located on O4 (O4O4′ case). This behavior has already been commented on for the HCHA-11/1 case (section 3.B). Irrespective of the lower Si/Al ratio, the H_2 molecule is at about the same distance (~2.0 Å) from the acidic proton as in the HCHA-11/1 case. In agreement with these results, the influence of the hydrogen molecule on the O−H stretching frequencies was noted only for the proton−oxygen pairs belonging to Al-I. As expected, a bathochromic shift was observed in most cases, except for O4O4′, where a minute hypsochromic shift was calculated (see data of Table 5). The strongest interaction was identified with the O2 position in the O2O2′ case. As far as the change of the H_2 stretching frequency is concerned, a bathochromic shift was computed in all of the studied combinations. Even if no clear correlation between the BE_c and the O−H and H−H frequency shift occurs, inspection of data in Table 5 reveals some surprising results;

TABLE 5: Optimized Distances between the H_2 Center of Mass and the Proton Site $d_{H\cdots H_2}$, BSSE-Corrected Binding Energies (BE_c), and Changes in the O−H Bond Distances and O−H and H−H Fundamental Stretching Frequencies for Each Combination of Brönsted Sites in HCHA-5/1 Zeolite[a]

			set of Al-I				set of Al-II					
			O−H bond				O−H bond				H−H bond	
combination	$d_{H\cdots H_2}$	BE_c	d_{OH}	Δd_{OH}	ω_{01}	$\Delta\omega_{01}$[b]	d_{OH}	Δd_{OH}	ω_{01}	$\Delta\omega_{01}$[b]	ω_{01}	$\Delta\omega_{01}$[c]
O1O4′	2.0511	2.2	0.9739	0.002	3584	−81	0.9735	0.000	3632	−2	4162	−76
O2O2′	2.1130	2.4	0.9731	0.003	3643	−56	0.9710	0.000	3700	1	4184	−54
O3O2′	2.0200	0.0	0.9777	0.002	3578	−69	0.9713	0.000	3641	1	4190	−48
O3O4′	2.0716	0.1	0.9758	0.002	3600	−64	0.9755	0.000	3622	0	4181	−57
O4O4′	2.0870	0.0	0.9711	−0.004	3617	+3	0.9750	0.000	3614	−1	4206	−32

[a] Distances are in angstroms, BE_c in kJ/mol, and frequencies and shifts in cm^{-1}. [b] For the O−H bond $\Delta\omega_{01}$ is defined by the difference: $\omega_{01}^{OH}{}_{[H_2-HCHA-5/1]} - \omega_{01}^{OH}{}_{[HCHA-5/1]}$. [c] For the H−H bond $\Delta\omega_{01}$ is defined by the difference: $\omega_{01}^{HH}{}_{[H_2-HCHA-5/1]} - \omega_{01}^{HH}{}_{[H_2]}$.

for the O3O2′, O3O4′, and O4O4′ cases, at variance with an almost zero BE_c both O−H and H−H frequencies undergo rather significant shifts. The reason is that the BSSE and kinetic barriers prevent the H_2 molecule from escaping from the chabazite cavity, so that some mutual influence between the electric field of the Brönsted site and the hydrogen molecule multipoles brings about some perturbation in the O−H and H−H force constants.

To detect possible cooperative effects resulting from higher hydrogen loadings, a second H_2 molecule was added in the cavity. Only the O2O2′ case was considered, being the site with the highest binding energy over the five possibilities (Table 5). The optimized geometry corresponds to each H_2 molecule independently in contact with each acidic site. The value of the BE_c for the double H_2 interaction is 4.7 kJ/mol, practically coinciding with the sum of the BE_c computed for the 1:1 complexes, for which values of about 2.4 kJ/mol were obtained (see the O2O2′ case in Table 5). As expected the two H_2 molecules adsorb almost in a Langmuirian manner (one molecule per proton site).

In a further step, the ONIOM2(MP2:B3LYP) approach was applied using as a model system the fragment shown in Figure 4b. The BE_c value per hydrogen molecule increases to 4.8 and 5.3 kJ/mol for the aug-cc-pVDZ and aug-cc-pVTZ basis sets, respectively, showing again a sizable contribution of dispersive forces.

4. Conclusions

In this work the ab initio B3LYP approach has been used to characterize the Al-substituted chabazite with a variable Si/Al ratio and to study the interaction of HCHA-11/1 and HCHA-5/1 (Si/Al ratios of 11/1 and 5/1, respectively) with molecular hydrogen. The main results are summarized in the following: (i) The Al content and its distribution have a relevant importance for the structure and the acidity of the HCHA. (ii) The relative stability of the proton sites in HCHA-11/1 confirmed the observation of two main peaks in the IR spectrum.[41] The two most stable positions present very similar frequencies that should represent the most abundant peak. The second peak would be attributed to the proton positioned in O4. The computed difference between the two peaks is around 30 cm^{-1} in good agreement with the 32 cm^{-1} reported by Bordiga et al.[41] (iii) For the H_2 interacting with HCHA-11/1, the BSSE-corrected binding energies are underestimated with respect to the experimental value. However, the obtained red shifts of the OH stretching frequencies are overestimated. This is possibly caused by a deficiency in the adopted level of theory. A ONIOM2 approach was applied to include dispersive interactions, at the MP2 level of theory, in the binding energy. For the most exposed O1 protonation site, this correction results in doubling the pure B3LYP binding energy. (iv) In the case of the interaction of the molecular hydrogen with HCHA-5/1, two sets of protonic sites were defined (one for each aluminum atom). All the possible Brönsted acidic proton locations were tested, and five cases were analyzed as far as the H_2 binding energy is concerned. A single molecule of H_2 preferred to locate itself close to only one extraframework proton letting the second free. This permits the addition of an extra H_2 molecule. It was observed by calculating their binding energies that the two molecules are independent, so the adsorption follows a Langmuirian behavior. The ONIOM2(MP2:B3LYP) approach was applied for the O2O2′ case. As in the HCHA-11/1 system, the binding energy increases its value twice approximately. Contrary to recent results[44] no correlation was found between the stretching frequency and the bond length of the adsorbed H_2 molecule.

In conclusion, our calculations confirm that the interaction between H_2 and the Brönsted site in acidic chabazites is weak and localized to the adsorption site. We believe that even if more accurate post-HF techniques (e.g., CCSD(T)) are adopted, at least in the proposed ONIOM2 scheme, the computed binding energy would still be below 8 kJ/mol. It is also expected that a further increase of the loading of aluminum in the unit cell (i.e., the number of Brönsted sites) would not change the adsorption capacity significantly. This is in line with a recent theoretical work[45] on the storage of hydrogen by encapsulation in a zeolitic framework. By means of molecular mechanics calculations with well-tailored pair potentials, it was shown that a maximum of 2.6 weight of hydrogen can be stored in the chabazite framework, which is well below the accepted target for mobile applications. Despite this, zeolites still deserve further investigation as hydrogen storage materials because of their possible use in fixed plants or in separation processes (e.g., to separate hydrogen from other gases). In this respect, the presence of more polarizing sites (e.g., alkali metal ions, transition metal ions) in the framework could lead to an improvement in the hydrogen storage capacity. Further work is necessary, and a study is in progress to characterize the interaction of molecular hydrogen with alkali-substituted CHAs.

Acknowledgment. F.J.T. acknowledges Regione Piemonte for his Ph.D. grant (Ab initio Simulation of the Hydrogen Storage Process in Microporous Materials).

References and Notes

(1) Chow, J.; Kopp, R. J.; Portney, P. R. *Science* **2003**, *302*, 1528−1531.

(2) Hoffert, M. I.; Caldeira, K.; Benford, G.; Criswell, D. R.; Green, C.; Herzog, H.; Jain, A. T.; Kheshgi, H. S.; Lackner, K. S.; Lewis, J. S.; Lightfoot, H. D.; Manheimer, W.; Mankins, J. C.; Mauel, M. E.; Perkins, L. J.; Schlesinger, M. E.; Volk, T.; Wigley, T. M. *Science* **2002**, *298*, 981−987.

(3) Vogel, G. *Science* **2004**, *305*, 966−967.
(4) Turner, J. *Science* **2004**, *305*, 972−974.
(5) Turner, J. *Science* **1999**, *285*, 687−689.
(6) Crabtree, G.; Dresselhaus, M.; Buchanan, M. *Phys. Today* **2004**, 39−44.
(7) Züttel, A. *Naturwissenschaften* **2004**, *91*, 157−172.
(8) Zecchina, A.; Bordiga, S.; Vitillo, J.; Ricchiardi, G.; Lamberti, C.; Spoto, G. *J. Am. Chem. Soc.* **2005**, *127*, 6361−6366.
(9) Weitkamp, J.; Fritz, M.; Ernst, S. *Int. J. Hydrogen Energy* **1995**, *20*, 967−970.
(10) Kazansky, V.; Borovkov, V.; Serich, A.; Karge, H. *Microporous Mesoporous Mater.* **1998**, *22*, 251−259.
(11) Makarova, M. A.; Zholobenko, V. L.; Al-Ghefaili, K. M.; Thompson, N. E.; Dewin, J.; Dwyer, J. *J. Chem. Soc., Faraday Trans.* **1994**, *90*, 1047−1054.
(12) Otero, C.; Manoilova, O. V.; Bonelli, B.; Rodr×c1guez, M.; Palomino, G. T.; Garrone, E. *Chem. Phys. Lett.* **2003**, *370*, 631−635.
(13) Baerlocher, C.; Meier, W.; Olson, D. *Atlas of Zeolite Framework Types*, 5th ed.; Elsevier: Amsterdam, The Netherlands, 2001.
(14) Diaz-Cabanas, M.; Barret, P.; Camblor, M. *Chem. Commun.* **1998**, 1881.
(15) Smith, L.; Davidson, A.; Cheetman, A. *Catal. Lett.* **1997**, *49*, 143−146.
(16) Paukshtis, E.; Soltanov, R.; Yurchenko, N. *React. Kinet. Catal. Lett.* **1981**, *16*, 93−96.
(17) Spoto, G.; Gribov, E.; Ricchiardi, G.; Damin, A.; Scarano, D.; Bordiga, S.; Lamberti, C.; Zecchina, A. *Prog. Surf. Sci.* **2004**, *76*, 71−146.
(18) Gale, J. *The General Utility Lattice Program (GULP)*; 1992−1994.
(19) Gale, J. *J. Chem. Soc., Faraday Trans.* **1997**, *93*, 629−637.
(20) Woodley, S.; Battle, P.; Gale, J.; Richard, C. *Phys. Chem. Chem. Phys.* **1999**, *1*, 2535−2542.
(21) Woodley, S.; Battle, P.; Gale, J.; Richard, C. *Phys. Chem. Chem. Phys.* **2004**, *6*, 1815−1822.
(22) Sierka, M.; Sauer, J. *Faraday Discuss.* **1997**, *106*, 41−62.
(23) Saunders, V. R.; Dovesi, R.; Roetti, C.; Orlando, R.; Zicovich-Wilson, C. M.; Harrison, N. M.; Doll, K.; Civalleri, B.; Bush, I. J.; D'Arco, P.; Llunell, M. *CRYSTAL03 User's Manual*; Università di Torino: Torino, 2003.
(24) Schlegel, H. B. *J. Comput. Chem.* **1982**, *3*, 214−218.
(25) Civalleri, B.; D'Arco, P.; Orlando, R.; Saunders: V. R.; Dovesi, R. *Chem. Phys. Lett.* **2001**, *348*, 131−138.
(26) Becke, A. D. *J. Chem. Phys.* **1993**, *98*, 5648.
(27) Koch, W.; Holthausen, M. C. *A Chemist's Guide to Density Functional Theory*; Wiley-VCH Verlag GmbH: Weinheim, Germany, 2000.
(28) Pascale, F.; Tosoni, S.; Zicovich-Wilson, C.; Ugliengo, P.; Orlando, R.; Dovesi, R. *Chem. Phys. Lett.* **2004**, *396*, 308−315.
(29) Ugliengo, P.; Busco, C.; Civalleri, B.; Zicovich-Wilson, C. M. *Mol. Phys.* **2005**, *103*, 2559−2571.
(30) Ugliengo, P. *Anharm: A Program To Solve the One-Dimensional Nuclear Schroedinger Equation*; 1989.
(31) Boys, S.; Bernardi, F. *Mol. Phys.* **1970**, *19*, 553.
(32) Krystyan, S.; Pulay, P. *Chem. Phys. Lett.* **1994**, *229*, 175−180.
(33) Pérez-Jorda, J.; Becke, A. *Chem. Phys. Lett.* **1995**, *233*, 134−137.
(34) Wu, Q.; Yang, W. *J. Chem. Phys.* **2002**, *116*, 515−524.
(35) Dapprich, S.; Komáromi, I.; Byun, K. S.; Morokuma, K.; Frisch, M. J. *J. Mol. Struct. (THEOCHEM)* **1999**, *461*, 1−21.
(36) Ugliengo, P.; Damin, A. *Chem. Phys. Lett.* **2002**, *366*, 683−690.
(37) Møller, C.; Plesset, M. *Phys. Rev.* **1934**, *46*, 618−622.
(38) Dunning, T. *J. Chem. Phys.* **1989**, *90*, 1007−1023.
(39) Frisch, M. J.; Trucks, G. W.; Schlegel, H. B.; Scuseria, G. E.; Robb, M. A.; Cheeseman, J. R.; Montgomery, J. A., Jr.; Vreven, T.; Kudin, K. N.; Burant, J. C.; Millam, J. M.; Iyengar, S. S.; Tomasi, J.; Barone, V.; Mennucci, B.; Cossi, M.; Scalmani, G.; Rega, N.; Petersson, G. A.; Nakatsuji, H.; Hada, M.; Ehara, M.; Toyota, K.; Fukuda, R.; Hasegawa, J.; Ishida, M.; Nakajima, T.; Honda, Y.; Kitao, O.; Nakai, H.; Klene, M.; Li, X.; Knox, J. E.; Hratchian, H. P.; Cross, J. B.; Bakken, V.; Adamo, C.; Jaramillo, J.; Gomperts, R.; Stratmann, R. E.; Yazyev, O.; Austin, A. J.; Cammi, R.; Pomelli, C.; Ochterski, J. W.; Ayala, P. Y.; Morokuma, K.; Voth, G. A.; Salvador, P.; Dannenberg, J. J.; Zakrzewski, V. G.; Dapprich, S.; Daniels, A. D.; Strain, M. C.; Farkas, O.; Malick, D. K.; Rabuck, A. D.; Raghavachari, K.; Foresman, J. B.; Ortiz, J. V.; Cui, Q.; Baboul, A. G.; Clifford, S.; Cioslowski, J.; Stefanov, B. B.; Liu, G.; Liashenko, A.; Piskorz, P.; Komaromi, I.; Martin, R. L.; Fox, D. J.; Keith, T.; Al-Laham, M. A.; Peng, C. Y.; Nanayakkara, A.; Challacombe, M.; Gill, P. M. W.; Johnson, B.; Chen, W.; Wong, M. W.; Gonzalez, C.; Pople, J. A. *Gaussian 03*, revision B.05; Gaussian, Inc.: Wallingford, CT, 2004.
(40) Zecchina, A.; Spoto, G.; Bordiga, S. *Phys. Chem. Chem. Phys.* **2005**, *7*, 1627−1642.
(41) Bordiga, S.; Regli, L.; Cocina, D.; Lamberti, C.; Bjørgen, M.; Lillerud, K. *J. Phys. Chem. B* **2005**, *109*, 2779−2784.
(42) Civalleri, B.; Garrone, E.; Ugliengo, P. *J. Phys. Chem. B* **1998**, *102*, 2373−2382.
(43) Lochan, R. C.; Head-Gordon, M. *Phys. Chem. Chem. Phys.* **2006**, *8*, 1357−1370.
(44) Benco, L.; Bucko, T.; Hafner, J.; Toulhoat, H. *J. Phys. Chem. B* **2005**, *109*, 22491−22501.
(45) Vitillo, J. G.; Ricchiardi, G.; Spoto, G.; Zecchina, A. *Phys. Chem. Chem. Phys.* **2005**, *7*, 3948−3954.